Dyes and Pigments 184 (2021) 108854

Contents lists available at ScienceDirect

Dyes and Pigments

journal homepage: http://www.elsevier.com/locate/dyepig

Iodinated xanthene-cyanine NIR dyes as potential photosensitizers for antimicrobial photodynamic therapy

T.M. Ebaston [a], Faina Nakonechny [b], Efrosiniia Talalai [a], Gary Gellerman [a], Leonid Patsenker [a,*]

[a] Department of Chemical Sciences, The Faculty of Natural Sciences, Ariel University, Ariel, 40700, Israel
[b] Department of Chemical Engineering, The Faculty of Engineering, Ariel University, Ariel, 40700, Israel

ARTICLE INFO

Keywords:
Xanthene-cyanine dye
Iodinated dye
Photosensitizer
Antimicrobial photodynamic therapy
APDT
Staphylococcus aureus

ABSTRACT

Photosensitizers (PSs) are chemical entities that upon light exposure are able to produce cytotoxic species such as singlet oxygen superoxide and free radicals. PSs are used in photodynamic therapy applications (PDT) to eradicate cancer cells, pathogenic bacteria, fungi, and viruses. Development of the NIR-activatable photosensitizes with high phototoxicity and low toxicity in dark conditions is challenging. Here we first report on the synthesis and antimicrobial testing of the new NIR photosensitizers based on the iodinated xanthene-cyanine dyes. These new photosensitizers exhibit high antimicrobial efficacy on *Staphylococcus aureus* pathogens at low dye concentration (~0.5 μM) and low NIR light dose (24.3 J/cm^2).

1. Introduction

Recently, the synthesis and spectral properties of several xanthene-cyanine dyes with a core structure shown in Fig. 1, A were reported [1]. These dyes absorb (679 nm) and emit light (705 nm) within the near-IR (NIR) spectral region, which is beneficial for probing in biological systems, in particular *in vivo*. Due to the high brightness (high extinction coefficients and fluorescence quantum yields), these dyes were proposed for biological sensing and imaging applications [2,3]. Several fluorogenic dyes with activatable emission have been developed based on the xanthene-cyanine core and evaluated as fluorescent reporters for targeted anticancer drug delivery monitoring [1] and other numerous imaging applications such as determination of hepatoxicity [4], activity of alkaline phosphatase [5], azoreductase [6] and leucine aminopeptidase [7], detection of cysteine [8] and keloid [9], imaging of biological nitroxyl [10] and hydrogen polysulphides [11], glutathione (GSH) activated cancer imaging [12], monitoring of thiol flux [13], photoacoustic visualization of peroxynitrite [14], probing of cancer specific enzyme hNQO1 [15], hypochlorous acid recognition [16], and pH sensing imaging *in vivo* [17]. However, phototoxicity of xanthene-cyanines on biological specimens has never been investigated, although this parameter seriously limits suitability of the dyes as the fluorescent reporters *in vitro* and *in vivo* [18]. Nevertheless, phototoxicity is a mandatory feature for photosensitizers (PSs) used in photodynamic therapy (PDT) applications [19–21].

The main goal of this work is to evaluate phototoxicity of the parent xanthene-cyanine dye **XCy** (Fig. 1,B) and explore possibility of developing highly phototoxic PSs based on this structure. One of the known methods to increase photosensitizing efficacy and phototoxicity of organic dyes is the introduction of heavy atoms such as iodine [22]. This approach has recently been demonstrated in the example of cyanine [23] and squaraines [24] dyes.

Herein, we report on the synthesis, spectroscopic characterization and phototoxicity of the new NIR-excitable mono- (**I-XCy**) and di-iodinated (**I_2-XCy**) xanthene-cyanine dyes (Fig. 1,B) *versus* the parent non-halogenated xanthene-cyanine **XCy** and FDA approved [25–27] heptamethine cyanine photosensitizer **ICG** [28], which is also activatable in the NIR range.

Phototoxicities of **XCy**, **I-XCy**, **I_2-XCy**, and **ICG** were tested on gram-positive *Staphylococcus aureus* (*S. aureus*) bacteria, which is a major human pathogen that causes a wide range of clinical infections. *S. aureus* can be commonly found on the skin and nose in most humans and can lead to death when entering bloodstream, joints, bones, lungs or heart [29]. Treatment usually involves antibiotics and drainage of the infected area. However, some staphylococcal infections no longer respond to common antibiotics [30] and antibacterial photodynamic therapy (APDT) is, therefore, an alternative beneficial method for eradication of this pathogen [31].

* Corresponding author. author.
E-mail addresses: ebaston@ariel.ac.il (T.M. Ebaston), fainan@ariel.ac.il (F. Nakonechny), ftalalay@gmail.com (E. Talalai), garyg@ariel.ac.il (G. Gellerman), leonidpa@ariel.ac.il (L. Patsenker).

https://doi.org/10.1016/j.dyepig.2020.108854
Received 9 May 2020; Received in revised form 26 July 2020; Accepted 11 September 2020
Available online 14 September 2020

2. Experimental

2.1. General

All chemicals were supplied by Alfa Aesar Israel and Sigma-Aldrich. 2,3,3-Trimethylindolenine (**2a**) was purchased from Aldrich and used as is. Solvents were purchased from Bio-Lab Israel and used as is. Chemical reactions were monitored by thin layer chromatography (TLC) (Silica gel 60 F-254, Merck) and by LC/MS.

LC/MS analysis was performed using an Agilent Technologies 1260 Infinity (LC) 6120 quadruple (MS), column Agilent SB-C18, 1.8 mm, 2.1 × 50 mm, column temperature 50 °C, eluent water-acetonitrile (ACN) + 0.1% formic acid.

HRMS was performed in ESI positive mode by using an Agilent 6550 iFunnel Q-TOF LC/MS instrument.

^{1}H NMR and ^{13}C NMR spectra were measured in CD_3OD at 300 K on a Bruker AvanceIII HD (^{1}H 400 MHz and ^{13}C 100 MHz) spectrometer and a BBO probe equipped with a Z gradient coil.

2.2. Synthesis

4-Iodophenylhydrazine 1b: Solution containing 4-iodoaniline (20 g, 91.3 mmol) and hydrochloric acid (5.5 M, 15 mL) was cooled to −10 °C and $NaNO_2$ (12.6 g, 182.6 mmol) in 45 mL of water was added dropwise with continuous stirring. The suspension was stirred for 30 min and then an ice-cold solution of $SnCl_2{\cdot}2H_2O$ (67.99 g, 301.3 mmol) in 40 mL of concentrated HCl was added dropwise keeping the temperature at −10 °C. The reaction mixture was stirred at that temperature for 1.5 h and then 18 h at 5 °C. The light brown precipitate was filtered and washed three times with water and extracted with ether. After drying over anhydrous $MgSO_4$, the ether layer was evaporated to dryness to afford **1b** as brown powder. Yield 17.94 g (84%). MS *m/z* (ESI^+) $C_6H_7IN_2$ calculated 233.96, found *m/z*: 233.90.

3,5-Diiodophenylhydrazine (1c): Phenyl hydrazine **1c** was obtained by the same procedure as for **1a** starting from 3, 5-diiodoaniline (5 g, 14.5 mmol) [32]. The product **1c** was isolated as fine brown needles. Yield 3.7 g, (72%). MS *m/z* (ESI^+) $C_6H_6I_2N_2$ calculated 359.86, found *m/z*: 359.9.

5-Iodo-2,3,3-trimethyl-3*H*-indole (**2b**) and 4,6-diiodo-2,3,3-trimethyl-3*H*-indole (**2c**) were prepared according to the literature procedure [33].

General procedure for the synthesis of 1,2,3,3-tetramethyl-3H-indolium (3a), 5-iodo-1,2,3,3-tetramethyl-3H-indolium (3b) and 4,6-diiodo-1,2,3,3-tetramethyl-3H-indolium (3c): 3a, 3b, 3c were synthesized according to the procedure [23]. Corresponding indolenine **2a–2c** (1 g, 500 mg and 500 mg, respectively, 6.3, 1.8 and 1.2 mmol) was dissolved in toluene (1 mL) and a large excess of methyl iodide (3 eq.) was added. The reaction mixture was heated in a pressure tube at 80 °C for 2 h, cooled to RT, and the precipitate was filtered and dried in a vacuum desiccator. Yields 760 mg (70%) (**3a**); 289 mg (55%) (**3b**); 222 mg (43%) (**3c**).

2-Chloro-3-(hydroxymethylene)cyclohex-1-ene-1-carbaldehyde (4) was synthesized according to the procedure [34].

2-(2-{2-Chloro-3-[2-(1,3,3-trimethyl-1,3-dihydro-indol-2-ylidene)-ethylidene]-cyclohex-1-enyl}-vinyl)-1,3,3-trimethyl-3*H*-indolium (5a): Catalytic amount of sodium acetate was added to a mixture of 2-chloro-3-hydroxymethylene-cyclohex-1-enecarbaldehyde (1 eq., 500 mg, 2.9 mmol) and 1,2,3,3-tetramethyl-3*H*-indolium **3a** (2.2 eq.,1.1 g, 6.38 mmol) in ethanol and stirred for 4 h at 50 °C at N_2 atmosphere. The resulting green solution was evaporated and purified by flash column chromatography using EtOAc/CH_3OH as eluent to afford compound **5a** as a dark green solid. Yield 900 mg (65%). MS *m/z* (ESI^+) $C_{32}H_{36}ClN_2^+$ calculated 483.25, found *m/z*: 483.0.

2-(2-{2-Chloro-3-[2-(5-iodo-1,3,3-trimethyl-1,3-dihydro-indol-2-ylidene)-ethylidene]-cyclohex-1-enyl}-vinyl)-5-iodo-1,3,3-trimethyl-3*H*-indolium (5b): Dye **5b** was synthesized from **3b** (2.2 eq., 43 mg, 0.14 mmol) according to the same procedure as **5a** affording a dark green solid. Yield 50 mg (47%). MS *m/z* (ESI^+) $C_{32}H_{34}ClI_2N_2^+$ calculated 735.05, found *m/z*: 735.1.

2-(2-{2-Chloro-3-[2-(4,6-diiodo-1,3,3-trimethyl-1,3-dihydro-indol-2-ylidene)-ethylidene]-cyclohex-1-enyl}-vinyl)-4,6-diiodo-1,3,3-trimethyl-3*H*-indolium (5c): Dye **5c** was synthesized from **3c** (2.2 eq., 108 mg, 0.25 mmol) according to the same procedure as **5a**. Dark green solid, yield 40 mg (35%). MS *m/z* (ESI^+) $C_{32}H_{32}ClI_4N_2^+$ calculated 986.84, found *m/z*: 986.8.

Dyes **5a–5c** were used for further synthesis without purification.

2-[2-(6-Hydroxy-2,3-dihydro-1*H*-xanthen-4-yl)-vinyl]-1,3,3-trimethyl-3H-indolium (XCy): Potassium carbonate (276 mg, 2 mmol) and resorcinol (220 mg, 2 mmol) were dissolved in acetonitrile (20 mL) and stirred for 15 min under N_2 atmosphere. The above mixture was added to a solution of **5a** (683 mg, 1 mmol) in acetonitrile (15 mL) and stirred for 8 h at 50 °C. The reaction was monitored by TLC. After the reaction was complete, the solvent was evaporated under reduced pressure and the crude product was column purified (silica gel 70–230 mesh, DCM—methanol, 90:10, v.v.). **XCy** was obtained as a blue solid. Yield 295 mg (61%). Purity 98% (LC/MS, 254 nm). ^{1}H NMR (400 MHz, CD_3OD): δ 8.64 (d, *J* = 16 Hz, 1H), 7.62 (d, *J* = 7.62 Hz, 1H), 7.51 (m, 2H), 7.40 (s, 1H), 7.32 (m, 2H), 6.74 (m, 2H), 6.33 (d, *J* = 16 Hz, 1H), 3.71 (s, 3H), 2.69 (t, *J* = 12 Hz, 2H), 2.62 (t, *J* = 12 Hz, 2H), 1.84 (m, 2H), 1.71 (s, 6H). ^{13}C NMR (100 MHz, CD_3OD): δ 164.64, 163.94, 146.11, 144.32, 137.29, 132.72, 130.88, 130.41, 128.03, 123.89, 117.31, 116.64, 116.05, 113.42, 103.74, 103.44, 100.62, 51.78, 32.71, 31.09, 30.26, 28.68, 25.47 MS *m/z* (ESI^+) $C_{26}H_{26}NO_2^+$ calculated 384.1964, found *m/z*: 384.1968.

2-[2-(6-Hydroxy-2,3-dihydro-1*H*-xanthen-4-yl)-vinyl]-5-iodo-1,3,3-trimethyl-3*H*-indolium (I-XCy): Dye **I-XCy** was synthesized similar to **XCy**, starting from **5b** (50 mg, 1 mmol). The product was isolated as a blue solid. Yield 15 mg (44%). Purity 80% (LC/MS 254 nm). ^{1}H NMR (400 MHz, CD_3OD): δ 8.59 (d, *J* = 16 Hz, 1H), 7.86 (s, 1H), 7.72 (dd, *J* = 8 Hz 1H), 7.45 (s, 1H), 7.36 (d, *J* = 8 Hz 1H), 7.13 (d, *J* = 8 Hz 1H), 6.76 (m, 2H), 6.23 (d, *J* = 16 Hz 1H), 3.62 (s, 3H), 2.70 (t, *J* = 12 Hz, 2H), 2.63 (t, *J* = 12 Hz, 2H), 1.93 (m, 2H), 1.69 (s, 6H). ^{13}C NMR (100 MHz, CD_3OD): δ 164.49, 157.07, 145.58, 145.17, 144.11, 139.73, 139.21, 138.32, 132.95, 131.01, 130.89, 126.89, 117.64, 116.73, 114.77, 103.24, 102.90, 90.77, 51.24, 36.70, 33.22, 32.34, 28.42, 23.89 MS *m/z* (ESI^+) $C_{26}H_{25}INO_2^+$ calculated 510.0930, found *m/z*: 510.0935.

2-[2-(6-Hydroxy-2,3-dihydro-1H-xanthen-4-yl)-vinyl]-4,6-diiodo-1,3,3-trimethyl-3H-indolium I_2-XCy: Dye **I_2-XCy** was synthesized similar to **XCy**, starting from **5c** (40 mg, 1 mmol). The product was

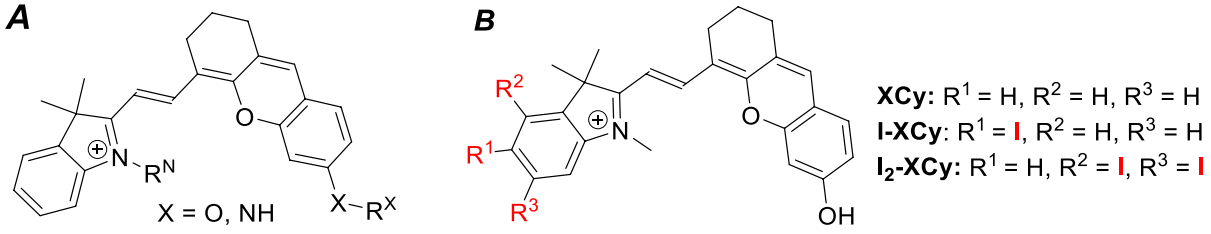

Fig. 1. Previously reported **XCy**-based dyes (***A***) and the dyes investigated in this work (***B***).

isolated as a blue solid. Yield 8 mg (32%). Purity 81% (LCMS, 254 nm). ^{1}H NMR (400 MHz, CD_3OD): δ 8.52 (d, $J = 16$ Hz, 1H), 7.94 (s, 1H), 7.60 (s, 1H), 7.52 (m, 1H), 7.41 (d, $J = 8$ Hz, 1H), 6.77 (m, 2H), 6.10 (d, $J = 12$ Hz 1H) 3.52 (s, 3H), 2.72 (t, $J = 12$ Hz, 2H), 2.64 (t, $J = 12$ Hz, 2H), 1.85 (m, 2H), 1.81 (s, 6H). ^{13}C NMR (100 MHz, CD_3OD): δ 157.4, 157.1, 155.3, 147.3, 146.2, 139.9, 137.3, 135.8, 131.0, 128.1, 119.6, 117.1, 116.4, 115.5, 108.7, 104.6, 96.2, 97.6, 51.0, 35.7, 33.2, 31.8, 29.9, 27.5, 25.1 MS *m/z* (ESI$^+$) $C_{26}H_{24}I_2NO_2^+$ calculated 635.9897, found *m/z*: 635.9810.

2.3. Absorption and fluorescence measurements

Absorption spectra were recorded on a Jasco V-730 UV–Vis spectrophotometer and the fluorescence spectra were taken on an Edinburgh FS5 spectrofluorometer. The absorption and fluorescence spectra were measured at 25 °C in standard 1-cm quartz cells at ~0.5 μM dye concentrations in 10 mM phosphate buffer pH 7.4 (PB) containing 5% methanol to facilitate solubility of the investigated compounds. Excitation wavelength (λ_{ex}) was 650 nm.

To determine the absolute fluorescence quantum yield (F_F), the integrated relative intensities were measured in PB *vs.* non-iodinated **XCy** dye in PB as the reference (F_F = 37%) [8], and the quantum yield was calculated according to Equation (1).

$$\Phi_F = \Phi_{FRef} \times (F / F_{Ref}) \times (A_{Ref} / A), \quad (1)$$

where Φ_{FRef} is the quantum yield of the reference, F_{Ref} and F are the areas (integral intensities) of the emission spectra ($F = \int I(\lambda)d\lambda$) of the reference dye and the dye under examination, A_{Ref} and A, are the absorbancies at the excitation wavelength of the reference and the dye under examination, respectively.

The quantum yield for each dye was independently measured three times and the average value was taken.

2.4. Antimicrobial studies

Culture of *S. aureus* (ATCC 25923) was grown on Brain Heart agar plates (BHA, Acumedia, Lansing, MI, USA) for 24 h, transferred into Brain Heart broth (BH, Acumedia, Lansing, MI, USA), grown at 37 ± 1 °C with shaking at 170 rpm until reaching the absorbance $A = 0.1$ at 660 nm, which corresponded to a final concentration of 10^8 cells/mL, and diluted then to the final concentration of 10^4–10^5 cells/mL.

All preparatory operations with photosensitizers were carried out in the dark to avoid their activation and photobleaching. The stock solutions of 0.1 mM of **XCy**, **I-XCy**, **I$_2$-XCy** and **ICG** in DMSO were prepared and the aliquots were added to 1 mL of *S. aureus* in BH to the final dye concentrations 0.1 μM, 0.5 μM and 1.0 μM. The amount of the DMSO dye solutions added to the bacteria suspensions did not exceed 0.5%. The cells were incubated in the dark for 15 min and then exposed to light for 5 min, 15 min and 30 min by a 660-nm, 12 W LED (light intensity 27 mW/cm^2; light dose 8.1 J/cm^2, 24.3 J/cm^2 and 48.6 J/cm^2, respectively).

After the light exposure, 100 μL aliquots of each sample at various decimal dilutions were spread over BHA plates with a Drigalsky spreader, incubated at 37 °C for 24 h, and the colony forming units (CFU) were counted by the *ImageJ* software [35]. To verify the dark toxicity of the dyes, the same experiments were carried out in parallel without light exposure. As the control we utilized the samples of *S. aureus* without dye (i) in the dark and without DMSO, (ii) in the dark in the presence of 1% DMSO, (iii) light irradiated without DMSO, and (iv) light irradiated in the presence of 1% DMSO.

All the experiments were carried out in triplicate and the average value was taken.

2.5. Fluorescence imaging

The fluorescence images were acquired by Photometrics CoolSNAP HQ2 camera mounted on an Olympus iX81 fluorescent microscope. The microscope was equipped with a 120 W metal halide discharge lamp. For the fluorescence images, a cube comprising an ET620/60x bandpass excitation filter, ET700/75 m bandpass emission filter and T66lpxr dichroic filter was used. All images were recorded with the same instrument settings. The images were taken with, exposure time 900 ms, gain 20 dB and × 20 magnification.

3. Results and discussion

3.1. Synthesis

We synthesized the known, non-iodinated xanthene-cyanine dye **XCy** [2] and its two new derivatives, mono-iodinated **I-XCy** and di-iodinated **I$_2$-XCy** (Scheme 1). The synthetic pathway was *via* the hydrazines **1a–1c** obtained as described in Ref. [32]. The hydrazines **1a–1c** were subjected to cyclocondensation with methyl-isopropyl ketone by the Fisher method to corresponding indolenines **2a–2c**. The last

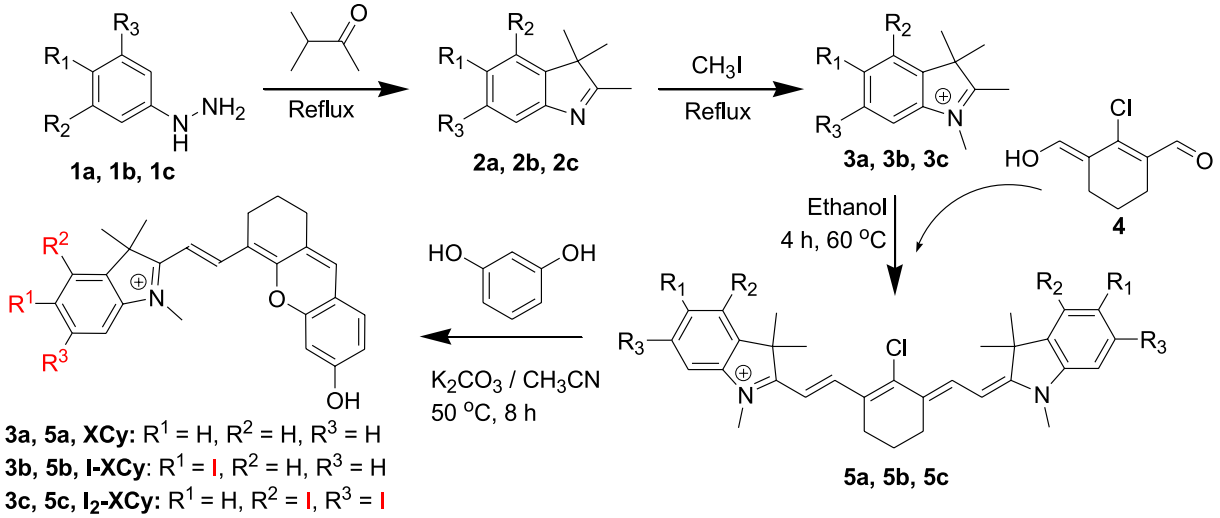

Scheme 1. Synthesis of **XCy**, **I-XCy** and **I$_2$-XCy** dyes.

ones were quaternized to indolenines **3a**–**3c** which were then reacted with cyclohexene carbaldehyde **4** to yield the intermediate chloro-cyanine dyes **5a**–**5c**, as described in Ref. [36]. The reported procedure was modified by using ethanol (solvent) instead of a mixture of dioxane and toluene (1:1), which allowed us to improve the synthetic yield and purity of the products. Cyanines **5a**–**5c** were then subjected to straightforward nucleophilic substitution of the chlorine atom with resorcinol to eliminate the indolenine moiety by a retro-Knovenagel reaction followed by cyclization and dehydration, as suggested in Ref. [2], to give the aimed xanthene-cyanines **XCy**, **I-XCy** and **I_2-XCy** in satisfactory yields (~40–60%).

3.2. Spectral properties

The spectral properties of **XCy**, **I-XCy** and **I_2-XCy** (c_{Dye} = 0.5 μM) were measured in phosphate buffer pH 7.4 (PB) containing 5% methanol to facilitate the dye solubility. All these dyes exhibit strong aggregation, which is observed as the broadened absorption bands and the violation of mirror symmetry between the absorption and fluorescence bands (Fig. 2). The aggregation predictably increases with increasing the number of iodine atoms. While the absorption (~680 nm) and emission (~705 nm) maxima for all these dyes are about the same, the extinction coefficients (ε) and the fluorescence quantum yields (Φ_F) noticeably decrease in the order: **XCy** > **I-XCy** > **I_2-XCy** (see Table 1).

Dyes **XCy**, **I-XCy** and **I_2-XCy** contain a conjugated hydroxyl group, which is subjected for protonation-deprotonation in respect to the solvent acidity. Obviously, the protonated and deprotonated forms possess different spectral properties and photosensitizing activity. In the example of the dye **XCy**, therefore, we investigated the pH dependent absorption and emission spectra. It can be seen that in the neutral (pH 7.4) and alkali (pH 11.0) media the dye exists preferably in the fluorescent deprotonated form with λ_{max}Ab ~ 679 nm and λ_{max}Fl ~ 705 nm (Fig. 3). In the acidic environment (pH 4.0), the absorption maximum is blue-shifted and the dye shows no detectable fluorescence. Importantly, in our further experiments the phototoxicities of the dyes are tested on the *S. aureus* bacteria, which have the intracellular pH in the range of 8.4–8.7 [37,] where the dyes exist mostly in the fluorescent deprotonated forms.

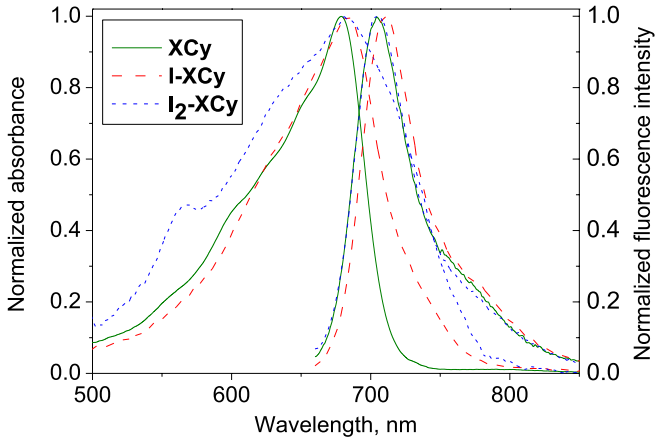

Fig. 2. Normalized absorption and emission spectra of **XCy** (solid line), **I-XCy** (dashed line) and **I_2-XCy** (dotted line) dyes (c_{Dye} = 0.5 μM) measured in 0.1 M PB pH 7.4 containing 5% methanol. λ_{ex} = 650 nm. T = 25 °C.

Table 1
Spectral properties of **XCy**, **I-XCy** and **I_2-XCy** (c_{Dye} = 0.5 μM) in phosphate buffer pH 7.4 (PB) containing 5% methanol: the absorption (λ_{max}Ab) and emission (λ_{max}Fl) maxima, extinction coefficient at the maximum (ε) and at 660 nm (ε_{660}), and the fluorescence quantum yield (Φ_F).

Dye	λ_{max}Ab, nm	ε (ε_{660}), $M^{-1}cm^{-1}$	λ_{max}Fl, nm	Φ_F, %
XCy	679	88,000 (71,000)	705	37
I-XCy	684	27,500 (23,300)	705	27
I_2-XCy	684	21,000 (18,700)	705	16
ICG	789	194,000 (18,400)	810	5

3.3. Antimicrobial activity

Our APDT experiments included the following three major steps (Scheme 2): (i) incubation of bacteria with PS in the dark (pre-irradiation incubation); (ii) irradiation of bacteria with various light doses (***a***) while, in parallel, bacteria were kept in the dark for the same time to be used as the reference (***b***); and (iii) growth of bacteria in the dark at 37 °C followed by the calculation of bacteria population.

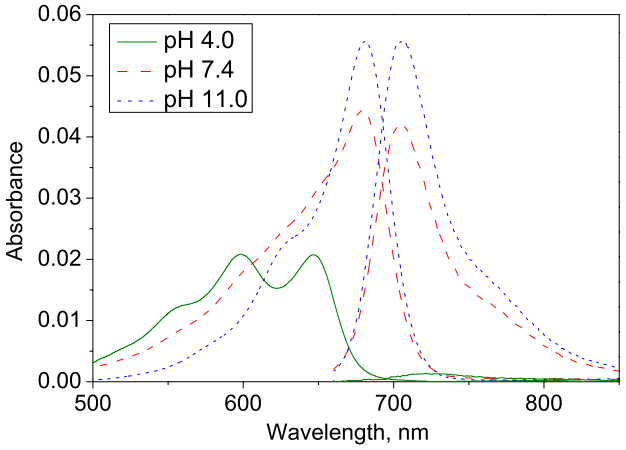

Fig. 3. Absorption and emission spectra of **XCy** (c_{Dye} = 0.5 μM) at pH 4.0 (solid line), 7.4 (dashed line) and 11.0 (dotted line). λ_{ex} = 650 nm. T = 25 °C. The fluorescence intensity at pH 11.0 is normalized to the absorption band at the same pH. The fluorescence intensities of the bands measured at pH 4.0 and pH 7.4 are shown relative to the fluorescence intensity of the band at pH 11.0.

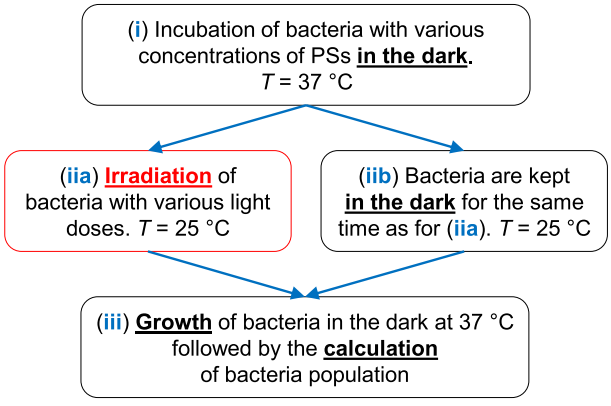

Scheme 2. APDT experiment.

First, we investigated the effect of the pre-irradiation incubation time (in the dark) on the PS uptake. For this, *S. aureus* bacteria were incubated with 1 μM **I_2-XCy** for 5, 15, 30 and 60 min, irradiated with 24.3 J/cm^2 light dose and cell survival was estimated (Fig. 4,A). It was found that even 5 min incubation is sufficient for the PS uptake. Nevertheless, in our further experiments we applied 15 min dark incubation to ensure the uptake of the dyes by cells. Because all the dyes are fluorescent, we were able to verify their uptake by using the fluorescence microscopy images acquired in 15 min after incubation. The corresponding images showing accumulation of the dyes in cells are presented in Fig. 5.

In the next step, the photodynamic eradication of *S. aureus* was investigated at three different PS concentrations (0.1, 0.5, 1.0 μM) and at three different light doses of 8.1 J/cm^2, 24.3 J/cm^2 and 48.6 J/cm^2 (5, 15, 30 min, respectively) using a 660-nm 12 W LED that produced 27 mW/cm^2 for each sample. The obtained results were compared to those for the **ICG** photosensitizer recently reported for its photodynamic eradication of *S. aureus in vitro* and *in vivo* [38–40]. It can be seen from the Table, that at the activation wavelength 660 nm, **ICG** absorbs about the same number of photons ($\varepsilon_{660} \sim 18{,}400\ M^{-1}cm^{-1}$) as **$I_2$-XCy** but this excitation is a bit less pronounced as compared to **I-XCy** ($\varepsilon_{660} \sim 23{,}300\ M^{-1}cm^{-1}$) and about four times smaller than that for **XCy** ($\varepsilon_{660} \sim 71{,}000\ M^{-1}cm^{-1}$). Nevertheless, in all our experiments **ICG** did not show a detectable eradication of *S. aureus* at least at a concentration of up to 1.0 μM and light dose of up to 48.6 J/cm^2, while **XCy**, **I-XCy** and **I_2-XCy** exhibit noticeable phototoxicity.

A comparative study of the investigated dyes demonstrates that their phototoxicity towards *S. aureus* noticeably increases with increasing the number of the iodine atoms: **XCy** < **I-XCy** < **I_2-XCy**. Thus, **I_2-XCy** exhibited the most significant eradication of *S. aureus* with only 1.1% cell survival at 1 μM and 24.3 J/cm^2 light dose; and almost no survival

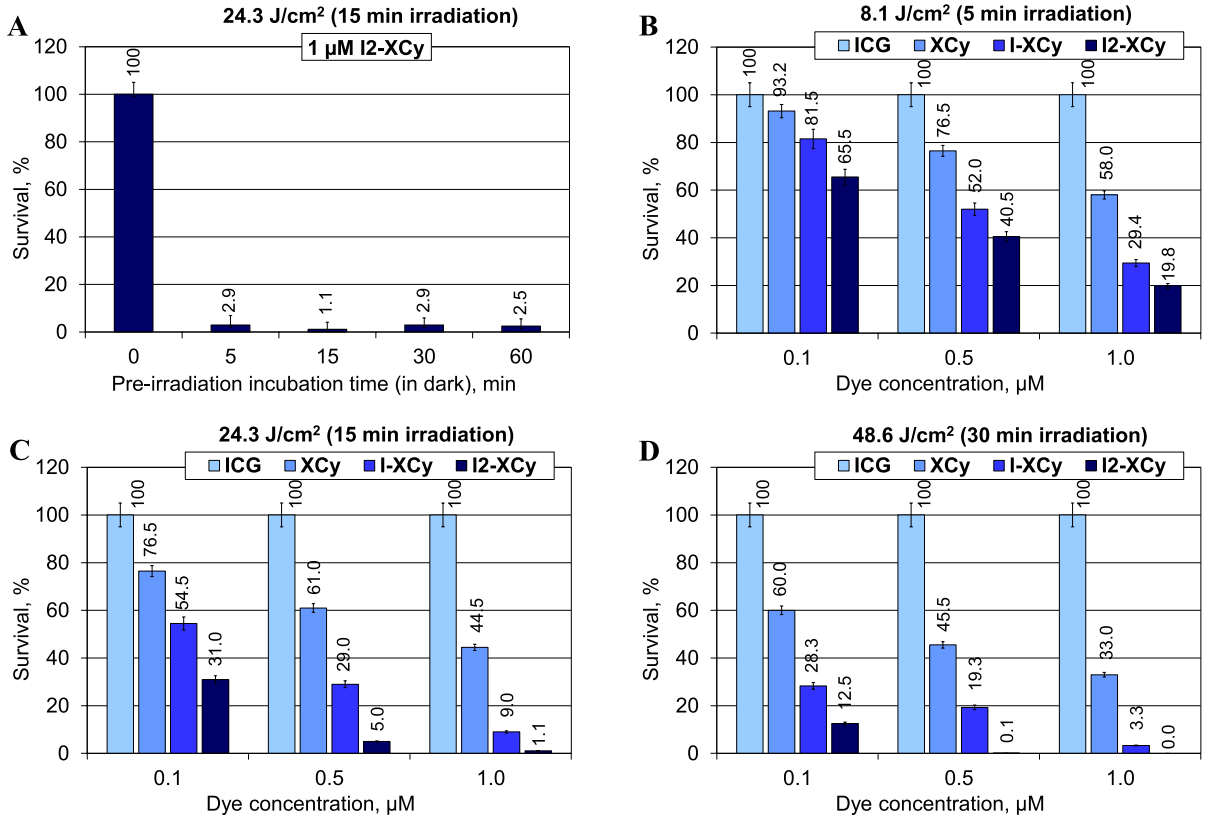

Fig. 4. APDT experiment. **A:** Effect of pre-irradiation incubation time on the *S. aureus* survival (step "**i**" on Scheme 2): **I_2-XCy** (1 μM) was incubated in the dark followed by a 24.3 J/cm^2 light exposure. **B–D** (step "**ii**" on Scheme 2)**:** *S. aureus* survival after 15 min of dark incubation followed by a 8.1 J/cm^2 (5 min, **B**), 24.3 J/cm^2 (15 min, **C**), and 48.6 J/cm^2 (30 min, **D**) light exposure. **ICG** (0.1–10 μM) does not eradicate *S. aureus* at the investigated light doses. Irradiation was performed by a 660-nm 12 W LED (27 mW/cm^2).

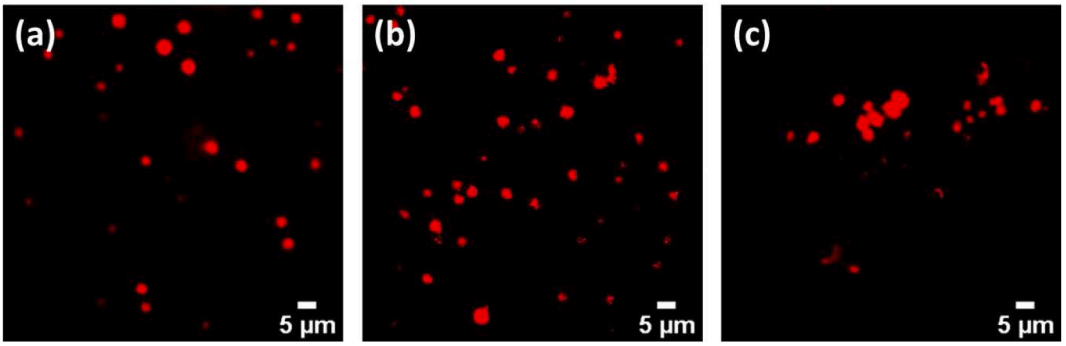

Fig. 5. Fluorescence microscopy images of *S. aureus* taken in 15 min dark incubation with 1 μM of **XCy** (**a**), **I-XCy** (**b**) and **I_2-XCy** (**c**).

cells were found at 0.5 μM and 48.6 J/cm^2 (Fig. 4,B–C). Remarkably, the reference dye **ICG** does not show any detectable eradication of *S. aureus* even at 10 μM concentration. Recently, **ICG** was reported to cause a pronounced eradication of *S. aureus* at 32 μM (25 μg/mL) and 100 J/cm^2 NIR light dose [38,39], which is a much more severe condition compared to those in our experiments. Importantly, all the investigated dyes were found to exhibit no dark toxicity to the bacteria at the concentrations of at least up to 10 μM.

4. Conclusions

The two iodinated xanthene-cyanine dyes **I-XCy** and **I$_2$-XCy** were synthesized, their spectral properties were investigated and the ability for the photoinduced eradication of *S. aureus* pathogens was studied in comparison with the non-iodinated xanthene-cyanine **XCy** and well established photosensitizer **ICG**. An increase in the number of iodine atoms was shown to enhance phototoxicity of the dyes. Due to the pronounced phototoxicity against *S. aureus* at low dye concentrations (0.5–1.0 μM), when irradiated with a low dose of NIR light (24.3–48.6 J/cm^2), low dark toxicity even at 10 μM, and sufficient brightness in the NIR region, the iodinated xanthene-cyanine dyes are considered promising photosensitizers for PDT applications.

CRediT authorship contribution statement

T.M. Ebaston: Experimental work: synthesis, spectroscopic characterization, photodynamic treatment, and fluorescence imaging. **Faina Nakonechny:** Supervision, and experimental work on the biological part of the research: Planning of biological experiments, cell culture preparation and cell analysis after the treatment. **Efrosiniia Talalai:** Experimental work: assistance in cell culture preparation and analysis of photodynamic treatment results. **Gary Gellerman:** Writing - original draft, Formulation of the problem, selection of the cells for the photodynamic experiments, and writing the article. **Leonid Patsenker:** Supervision, Writing - original draft, of the work in general, development of photosensitizers, planning synthetic, spectroscopic and photodynamic experiments, formulating conclusions, and writing the article.

Declaration of competing interest

The authors declare that they have no known competing financial interests or personal relationships that could have appeared to influence the work reported in this paper.

Acknowledgements

This work was supported by the Israel Scientific Foundation (ISF), project 810/18 and the Ariel University, Isreal (Joint Research Project between Ariel University and Florida Atlantic University), FAU project RA2000000056. Leonid Patsenker is thankful to the Center for Absorption in Science of the Ministry of Immigrant Absorption of Israel for the financial support under the KAMEA program. Gary Gellerman is thankful to the Gale Foundation for the generous donation to support this work.

Appendix A. Supplementary data

Supplementary data to this article can be found online at https://doi.org/10.1016/j.dyepig.2020.108854.

References

[1] Ebaston TM, Rozovsky A, Zaporozhets A, Bazylevich A, Tuchinsky H, Marks V, Gellerman G, Patsenker L. Peptide-driven targeted drug delivery system comprising turn-on near-infrared fluorescent xanthene–cyanine reporter for real-time monitoring of drug release. ChemMedChem 2019;14:1727–34. https://doi.org/10.1002/cmdc.201900464.

[2] Yuan L, Lin W, Zhao S, Gao W, Chen B, He L. A unique approach to development of near-infrared fluorescent sensors for in vivo imaging. J Am Chem Soc 2012;134:13510–23. https://doi.org/10.1021/ja305802v.

[3] Ong H, Debieu S, Moreau M, Romieu A, Richard JA. Synthesis of N,N-Dialkylamino-nor-dihydroxanthene-hemicyanine fused near-infrared fluorophores and their first water-soluble and/or bioconjugatable analogues. Chem Asian J 2017;12:936–46. https://doi.org/10.1002/asia.201700176.

[4] Cheng P, Miao Q, Li J, Huang J, Xie C, Pu K. Unimolecular chemo-fluoro-luminescent reporter for crosstalk-free duplex imaging of hepatotoxicity. J Am Chem Soc 2019;141:10581–4. https://doi.org/10.1021/jacs.9b02580.

[5] Tan Y, Zhang L, Man KH, Peltier R, Chen G, Zhang H. Reaction-based off–on near-infrared fluorescent probe for imaging alkaline phosphatase activity in living cells and mice. ACS Appl Mater Interfaces 2017;9:6796–803. https://doi.org/10.1021/acsami.6b14176.

[6] Tian Y, Li Y, Jiang WL, Zhou DY, Fei J, Li CY. In-Situ imaging of azoreductase activity in the acute and chronic ulcerative colitis mice by a near-infrared fluorescent probe. Anal Chem 2019;91. https://doi.org/10.1021/acs.analchem.9b02857. 10901–7.

[7] He X, Li L, Fang Y, Shi W, Li X, Ma H. In vivo imaging of leucine aminopeptidase activity in drug-induced liver injury and liver cancer via a near-infrared fluorescent probe. Chem Sci 2017;8:3479–83. https://doi.org/10.1039/c6sc05712h.

[8] Han C, Yang H, Chen M, Su Q, Feng W, Li F. Mitochondria-targeted near-infrared fluorescent off-on probe for selective detection of cysteine in living cells and in vivo. ACS Appl Mater Interfaces 2015;7:27968–75. https://doi.org/10.1021/acsami.5b10607.

[9] Miao Q, Yeo DC, Wiraja C, Zhang J, Ning X, Xu C. Near-Infrared fluorescent molecular probe for sensitive imaging of keloid. Angew Chem 2018;130:1270–4. https://doi.org/10.1002/ange.201710727.

[10] Tan Y, Liu R, Zhang H, Peltier R, Lam YW, Zhu Q. Design and synthesis of near infrared fluorescent probes for imaging of biological nitroxyl. Sci Rep 2015;5:16979. https://doi.org/10.1038/srep16979.

[11] Fang Y, Chen W, Shi W, Li H, Xian M, Ma H. A near-infrared fluorescence off-on probe for sensitive imaging of hydrogen polysulfides in living cells and mice: in vivo. Chem Commun 2017;53:8759–62. https://doi.org/10.1039/c7cc04093h.

[12] Guo R, Huang F, Zhang B, Yan Y, Che J, Jin Y. GSH Activated biotin-tagged near-Infrared probe for efficient cancer imaging. Theranostics 2019;9:3515–25. https://doi.org/10.7150/thno.32742.

[13] Yang Y, Zhou T, Jin M, Zhou K, Liu D, Li X. Thiol–chromene "click" reaction triggered self-Immolative for NIR visualization of thiol flux in physiology and pathology of living cells and mice. J Am Chem Soc 2020;142:1614–20. https://doi.org/10.1021/jacs.9b12629.

[14] Zhang J, Zhen X, Zeng J, Pu K. A Dual-modal molecular probe for near-infrared fluorescence and photoacoustic imaging of peroxynitrite. Anal Chem 2018;90. https://doi.org/10.1021/acs.analchem.8b01879. 9301–7.

[15] Zhang C, Zhai BB, Peng T, Zhong Z, Xu L, Zhang QZ. Design and synthesis of near-infrared fluorescence-enhancement probes for the cancer-specific enzyme hNQO1. Dyes Pigments 2017;143:245–51. https://doi.org/10.1016/j.dyepig.2017.04.043.

[16] Ma J, Yan C, Li Y, Duo H, Li Q, Lu X. Unusual hypochlorous acid (HClO) recognition mechanism based on chlorine–oxygen bond (Cl−O) formation. Chem Eur J 2019;25:7168–76. https://doi.org/10.1002/chem.201806264.

[17] Li Y, Wang Y, Yang S, Zhao Y, Yuan L, Zheng J. Hemicyanine-based high resolution ratiometric near-infrared fluorescent probe for monitoring pH changes in vivo. Anal Chem 2015;87:2495–503. https://doi.org/10.1021/ac5045498.

[18] Kiepas A, Voorand E, Mubaid F, Siegel PM, Brown CM. Optimizing live-cell fluorescence imaging conditions to minimize phototoxicity. J Cell Sci 2020;133:jcs242834. https://doi.org/10.1242/jcs.242834.

[19] Jenni S, Sour A. Molecular theranostic agents for photodynamic therapy (PDT) and magnetic resonance imaging (MRI). INORGA 2019;7:10. https://doi.org/10.3390/inorganics7010010.

[20] Ghorbani J, Rahban D, Aghamiri S, Teymouri A, Bahador A. Photosensitizers in antibacterial photodynamic therapy: an overview. Laser Ther 2018;27:293–302. https://doi.org/10.5978/islsm.27_18-RA-01.

[21] Pereira RL. Antimicrobial photodynamic therapy: a new therapeutic option to combat infections. J Med Microbiol Diagn 2014. https://doi.org/10.4172/2161-0703.1000158. 03.

[22] Changquan T, Ping H, En M, Mingdong H, Qingdong Z. Heavy atom enhanced generation of singlet oxygen in novel indenofluorene-based two-photon absorbing chromophores for photodynamic therapy. Dyes Pigments 2015;117:7–15. https://doi.org/10.1016/j.dyepig.2015.01.019.

[23] Jones GW, Tatarets AL, Patsenker LD. Halogenated compounds for photodynamic therapy. US 9572881; US 9095612; EP2850061; US 9040721; US8962797; US 8748446.

[24] Mandim F, Graça V, Calhelha RC, Ferreira LFV, Ferreira ICFR, Santos PF. Synthesis, photochemical and in vitro cytotoxic evaluation of new iodinated aminosquaraines as potential sensitizers for photodynamic therapy. Molecules 2019;24:863. https://doi.org/10.3390/molecules24050863.

[25] Filippi M, Garello F, Pasquino C, Arena F, Giustetto P, Antico F, Terreno E. Indocyanine green labeling for optical and photoacoustic imaging of mesenchymal stem cells after in vivo transplantation. J Biophot 2019;12(5):e201800035. https://doi.org/10.1002/jbio.201800035.

[26] Rychlik IE, Mehta HS. Review of revised label and labeling. Memorandum 2018. available from, https://www.accessdata.fda.gov/drugsatfda_docs/nda/2018/211580Orig1s000OtherR.pdf.

[27] Libero M, Marzella L. Multi-disciplinary review and evaluation. Spy agent green. NDA 211580 505(b)(2) available from: https://www.fda.gov/media/124115/download; 2018.

[28] Omar GS, Wilson M, Nair SP. Lethal photosensitization of wound-associated microbes using indocyanine green and near-infrared light. BMC Microbiol 2008;8:111. https://doi.org/10.1186/1471-2180-8-111.
[29] Tong SYC, Davis JS, Eichenberger E, Holland TL, Fowler VG. Staphylococcus aureus infections: epidemiology, pathophysiology, clinical manifestations, and management. Clin Microbiol Rev 2015;28:603–61. https://doi.org/10.1128/CMR.00134-14.
[30] Pantosti A, Sanchini A, Monaco M. Mechanisms of antibiotic resistance in Staphylococcus aureus. Future Microbiol 2007;2:323–34. https://doi.org/10.2217/17460913.2.3.323.
[31] Pérez-Laguna V, Pérez-Artiaga L, Lampaya-Pérez V, García-Luque I, Ballesta S, Nonell S. Bactericidal effect of photodynamic therapy, alone or in combination with mupirocin or linezolid, on Staphylococcus aureus. Front Microbiol 2017;8:1–9. https://doi.org/10.3389/fmicb.2017.01002.
[32] Bérubé M, Poirier D. Synthesis of simplified hybrid inhibitors of type 1 17β-hydroxysteroid dehydrogenase via cross-metathesis and sonogashira coupling reactions. Org Lett 2004;6:3127–30. https://doi.org/10.1021/ol048820u.
[33] Atchison J, Kamila S, Nesbitt H, Logan KA, Nicholas DM, Fowley C. Iodinated cyanine dyes: a new class of sensitisers for use in NIR activated photodynamic therapy (PDT). Chem Commun 2017;53. https://doi.org/10.1039/C6CC09624G. 2009–12.
[34] Prasad PR, Selvakumar K, Singh HB, Butcher RJ. Synthesis, structure, and bonding of 1-oxa-6,6aλ 4-chalcogenopentalenes and eelated derivatives; the role of intramolecular coordination. J Org Chem 2016;81:3214–26. https://doi.org/10.1021/acs.joc.6b00173.
[35] Rasband W. National Institutes of Health, USA. http://imagej.nih.gov/ij; 2020.
[36] Rozovsky A, Ebaston TM, Zaporozhets A, Bazylevich A, Tuchinsky H, Patsenker L, Gellerman G. Theranostic system for ratiometric fluorescence monitoring of peptide-guided targeted drug delivery. RSC Adv 2019;9:32656–64. https://doi.org/10.1039/C9RA06334J.
[37] Sannasiddappa TH, Lund PA, Clarke SR. In vitro antibacterial activity of unconjugated and conjugated bile salts on Staphylococcus aureus. Front Microbiol 2017 23;8:1581. https://doi.org/10.3389/fmicb.2017.01581.
[38] Wong TW, Liao SZ, Ko WC, Wu CJ, Wu SB, Chuang YC, Huang IH. Indocyanine green-mediated photodynamic therapy reduces methicillin-resistant *Staphylococcus aureus* drug resistance. J Clin Med 2019;8(3):411. https://doi.org/10.3390/jcm8030411.
[39] Wong TW, Wu EC, Ko WC, Lee CC, Hor LI, Huang IH. Photodynamic inactivation of methicillin-resistant Staphylococcus aureus by indocyanine green and near infrared light. Dermatol Sin 2018;36(1):8–15. https://doi.org/10.1016/j.dsi.2017.08.003.
[40] Li X, Huang W, Zheng X, Chang S, Liu C, Cheng Q, Zhu S. Synergistic in vitro effects of indocyanine green and ethylenediamine tetraacetate-mediated antimicrobial photodynamic therapy combined with antibiotics for resistant bacterial biofilms in diabetic foot infection. Photodiagnosis Photodyn Ther 2019;25:300–8. https://doi.org/10.1016/j.pdpdt.2019.01.010.